**Atmospheric
Chemistry
and Physics**

Measurements of cloud condensation nuclei activity and droplet activation kinetics of fresh unprocessed regional dust samples and minerals

P. Kumar[1], I. N. Sokolik[2], and A. Nenes[1,2]

[1]School of Chemical & Biomolecular Engineering, Georgia Institute of Technology, Atlanta, GA, 30332, USA
[2]School of Earth & Atmospheric Sciences, Georgia Institute of Technology Atlanta, GA, 30332, USA

Abstract. This study reports laboratory measurements of cloud condensation nuclei (CCN) activity and droplet activation kinetics of aerosols dry generated from clays, calcite, quartz, and desert soil samples from Northern Africa, East Asia/China, and Northern America. Based on the observed dependence of critical supersaturation, s_c, with particle dry diameter, D_{dry}, we found that FHH (Frenkel, Halsey and Hill) adsorption activation theory is a far more suitable framework for describing fresh dust CCN activity than Köhler theory. One set of FHH parameters ($A_{FHH} \sim 2.25 \pm 0.75$, $B_{FHH} \sim 1.20 \pm 0.10$) can adequately reproduce the measured CCN activity for all species considered, and also explains the large range of hygroscopicities reported in the literature. Based on a threshold droplet growth analysis, mineral dust aerosols were found to display retarded activation kinetics compared to ammonium sulfate. Comprehensive simulations of mineral dust activation and growth in the CCN instrument suggest that this retardation is equivalent to a reduction of the water vapor uptake coefficient (relative to that for calibration ammonium sulfate aerosol) by 30–80%. These results suggest that dust particles do not require deliquescent material to act as CCN in the atmosphere.

1 Introduction

Clouds are an important component of the Earth's radiation budget and hydrological cycle. Even small changes in cloud properties may have significant impacts on climate (Collins et al., 1994). Perturbations in aerosol loadings can alter cloud properties, giving rise to the aerosol indirect effect on climate. Aerosol effects on clouds constitute one of the most uncertain components of anthropogenic climate change (Forster et al., 2007). Mineral aerosol (or dust) is one of the lesser understood of aerosol species in the study of aerosol-cloud-climate interactions. It has been well recognized that dust plays an important role in cold cloud processes because of its effectiveness as Ice Nuclei (IN) (DeMott et al., 2003; Field et al., 2006). Dust can also affect warm clouds by acting as Cloud Condensation Nuclei (CCN), changes of which affect their radiative (Twomey, 1974) and precipitation properties (Rosenfeld et al., 2001).

In general, the ability of dust particles to serve as CCN depends on their mineralogy, size, morphology, and atmospheric processing. Quantitative understanding of the interactions of dust with water vapor is complex because of its varying source-dependent mineralogical composition and aging during its atmospheric residence. Mineral aerosol may constitute of iron oxides (e.g., hematite, goethite), carbonates (e.g., calcite, dolomite), quartz, and clays (e.g., kaolinite, illite, and montmorillonite) (Lafon et al., 2006; Chou et al., 2008; Coz et al., 2009; Twohy et al., 2009). Dust particles mainly originate from arid and semi-arid regions, with an annual emission of approximately 1000–5000 Tg (Schuttlefield et al., 2007). Differences in parent soils, and emission and transport processes cause substantial variability in size-resolved composition and morphology of dust particles (Sokolik et al., 2001; Jeong and Sokolik, 2007). Dust particles can remain suspended in the atmosphere for up to several weeks and can be transported over large distances downwind from source regions. During their transport, dust particles (especially the carbonate fraction which can comprise up to 30% of the total mass), provides reaction sites for heterogeneous chemical reactions with atmospheric trace gases and pollutants (Levin et al., 1996), resulting in modified dust properties, such as enhanced hygroscopicity (Hatch et al., 2008). However, not all dust particles undergo aging (Prospero, 1999; Ganor and Mamane, 1982; Ganor and Foner,

Correspondence to: A. Nenes
(athanasios.nenes@gatech.edu)

1996). Depending on transport routes of dust plumes and environmental conditions, dust particles can remain unprocessed and have the same properties as freshly emitted dust in source regions. Thus, it is important to understand the CCN activity of fresh dust particles as well as aged dust.

To describe the CCN activity of freshly emitted dust, two phenomena must be accounted for: (i) the effect of solute (which may be present in freshly emitted dust or formed during atmospheric aging), and (ii) the adsorption of water on the insoluble component of the dust particles. The former can be accounted for by using Köhler theory (KT) (Köhler, 1936) and the latter with adsorption activation theory (AT) (Henson, 2007; Sorjamaa and Laaksonen, 2007; Kumar et al., 2009a). The formulation of Henson (2007) used the BET (Brunauer et al., 1938) adsorption isotherm, while Sorjamaa and Laaksonen (2007) used the multilayer FHH (Frenkel, Halsey and Hill) adsorption isotherm with two adjustable parameters (A_{FHH} and B_{FHH}). Based on analysis of published data on dust-water interactions, Kumar et al. (2009b) showed the importance of including water adsorption effects when describing the hygroscopic and CCN behavior of mineral aerosol. The same study found that FHH particles require less water to activate to cloud droplets than particles activating by KT; this implies that the competition for water vapor by FHH particles is less intense that KT particles to form droplets with implications for parcel maximum supersaturation, s_{max}, and cloud droplet number, N_d. Kumar et al. (2009a) addressed the need to account for adsorption activation in atmospheric models by developing a cloud droplet formation parameterization where the CCN constitutes an external mixture of soluble aerosol (that follow KT) and insoluble aerosol (that follow FHH adsorption activation theory, FHH-AT). Here, we report new measurements to further support the dust-CCN parameterization developed by Kumar et al. (2009a).

Past studies have already demonstrated that both regional dusts as well as individual clays can interact with water and act as effective CCN. For example, Koehler et al. (2009) and Herich et al. (2009) measured CCN activation of two types of regional dust samples (Northern Africa and Arizona Test Dust) and several clays (kaolinite, illite, and montmorillonite), respectively, at water vapor supersaturation relevant to atmospheric conditions. These studies, however, parameterized the observed hygroscopicity using a KT framework in terms of a hygroscopicity parameter, κ (Petters and Kreidenweis, 2007). This approach was evaluated by Kumar et al. (2009b), who, after examining the relationship between s_c and D_{dry} for the published dust samples suggested that FHH-AT is a better description of fresh dust CCN activity as the s_c-D_{dry} exponents determined from FHH-AT were closer to observations than from KT. Furthermore, no study to date has accounted for non-sphericity effects in the CCN activity relationships, even when it is well known that dust particles are non-spherical (e.g., Okada et al., 2001; Chou et al., 2008). Further, the effect of multiple-charged particles in the electri-

cal mobility classification for measurements of size-resolved CCN activity (required for determining s_c and D_{dry}) is often addressed by removal of the secondary peaks in the activation curves (e.g., Lance et al., 2006; Rose et al., 2008). If multiple-charged particles are present in significant enough numbers (such as for dust CCN), this approach may not suffice causing biases in measured CCN activity towards higher hygroscopicity (Petters et al., 2007). A comprehensive analysis of charging efficiency (e.g., Moore et al., 2010) needs to be considered to avoid such biases in observed hygroscopicity.

In this study, we investigate the CCN-relevant properties of clays and several dust samples representative of major regional dust sources. Measurements were carried out with a Droplet Measurement Technologies Continuous-Flow Streamwise Thermal Gradient CCN (CFSTGC) counter (Roberts and Nenes, 2005; Lance et al., 2006). The CCN activation behavior of mineral aerosols generated from Northern American, African, and East Asian desert soils as well as individual clays (illite and montmorillonite), calcite ($CaCO_3$), and quartz (SiO_2) are studied. The effects of multiple charging and shape (non-sphericity) on the electrical mobility sizing of particles and activation curves are examined. The experimental results are used to infer the dominant activation physics (KT or FHH-AT) and determine the appropriate adsorption parameters (e.g., A_{FHH} and B_{FHH}) that describe the hygroscopicity of fresh dust for the use in droplet activation parameterizations of Kumar et al. (2009a). Finally, using the method of threshold droplet growth analysis (TDGA, e.g., Asa-Awuku et al., 2010; Padró et al., 2010), potential retardations in the activation kinetics of dust (compared to calibration aerosol) are identified. A comprehensive simulation of dust activation in the CCN instrument is then performed to parameterize these kinetic delays in terms of changes in the effective water vapor uptake coefficient.

2 Measurements and data analysis

2.1 Regional dust samples and individual minerals

Aerosols from regional soil samples and individual minerals/clays were generated and analyzed in this study. Table 1 provides a summary of the analyzed samples, including information on the location of sample collection. The soil samples were collected in source regions of Northern Africa and East Asia. Commercially available Arizona Test Dust (ATD) was used as representative of North America soil. Individual minerals/clays used to generate aerosol were analyzed as purchased, with no physical and chemical treatments to resemble atmospheric behaviors.
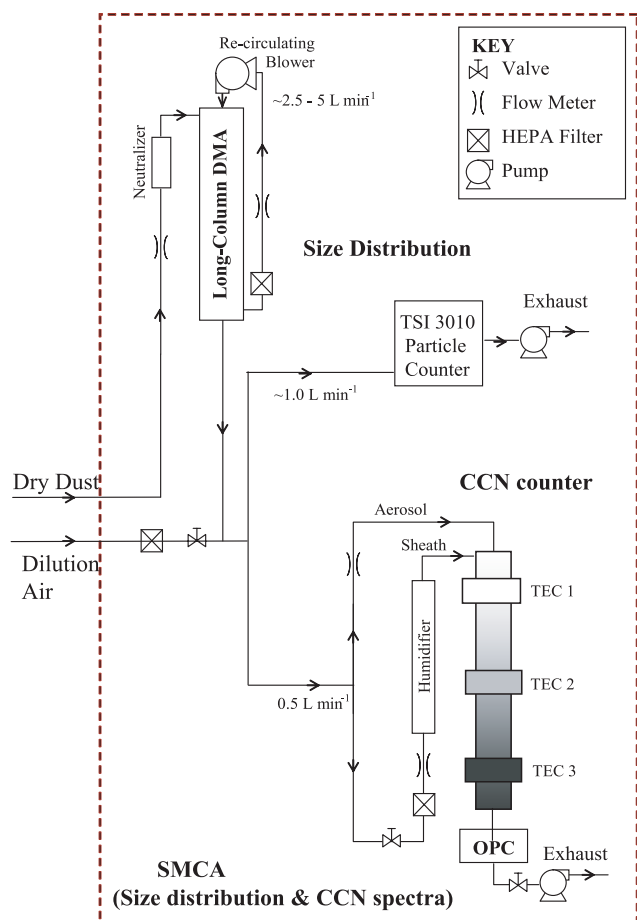
Fig. 1. Schematic of the experimental set-up used for size resolved CCN activation and droplet growth kinetics measurements.

2.2 Measurements of CCN activity

The measurement setup consists of three sections: aerosol generation, particle size selection, and CCN measurement (Fig. 1). To generate aerosol, approximately 3 g of the desired sample were placed in a 1000 ml sealed Erlenmeyer flask which is connected to a Burrell-Wrist Action Shaker (Model 75). Compressed filtered air is introduced into the flask that generates polydisperse fine aerosols by mechanical disintegration ("saltation") with a distribution that resembles the size distributions of dust plumes generated in the natural source regions (Lafon et al., 2006).

The dry aerosol is then sent to the electrostatic classifier for particle size selection (TSI Model 3080) with a Differential Mobility Analyzer (DMA, TSI Model 3081). Before entering the classifier, aerosols are passed through an impactor to remove supermicro-meter size particles (i.e., size greater than 1 µm) and then charged with a series of Kr-85 neutralizers. The particles are then classified in the DMA by their electrical mobility set by the voltage applied to the DMA. The Sheath flow rate in the DMA is set to $2.3\,1\,min^{-1}$,

and the monodisperse flow is set to $0.45\,1\,min^{-1}$. The classified aerosol flow is mixed with filtered air and then sampled by a Condensation Particle Counter (CPC, TSI Model 3010), and a Droplet Measurement Technologies Continuous Flow Streamwise Thermal Gradient CCN (CFSTGC) chamber.

The CPC measures the total concentration of aerosol, or condensation nuclei (CN) present in the monodisperse stream. The fraction of aerosol acting as CCN is measured by exposing particles to a constant water vapor supersaturation within the CFSTGC. This is done by flowing the aerosol in a cylindrical column with wetted walls upon which a thermal gradient, ΔT, is applied in the axial direction. The difference in diffusivity between water vapor and heat is exploited for the generation of water vapor supersaturation, s, which reaches maximum at the column centerline. CCN flowing along the column centerline are activated to cloud droplets and are counted at the exit with an optical particle counter (OPC). Each value of ΔT generates a unique supersaturation value, which in this study varied between 0.15% and 1%. CCN activity is characterized by the dry activation diameter, D_{dry}, which corresponds to the minimum dry particle diameter that activates at the certain supersaturation of interest, s_c. D_{dry} is found by expressing the ratio of CCN to CN concentration as a function of dry particle diameter, and, determining the diameter for which 50% of the classified aerosol acts as CCN.

The calibration of the instrument supersaturation is determined from the D_{dry} of $(NH_4)_2SO_4$ calibration aerosol at a given ΔT. $(NH_4)_2SO_4$ aerosol was generated by atomizing an aqueous solution and subsequently drying the droplet stream with a series of silica-gel diffusion dryers. D_{dry} of $(NH_4)_2SO_4$ is then related to s by applying Köhler theory, assuming that $(NH_4)_2SO_4$ has a shape factor of 1.04 in the DMA (Kuwata and Kondo, 2009), density of $1760\,kg\,m^{-3}$, surface tension of water (calculated at the average column temperature), molar mass of $0.132\,kg\,mol^{-1}$, and osmotic coefficients calculated with the Pitzer activity coefficient model (Pitzer and Mayorga, 1973). A relationship between ΔT vs. instrument supersaturation is determined by repeating the above calibration procedure over a range of ΔT. This relationship is then used in all dust activation experiments. Calibration is repeated throughout the measurements, and exhibits little variability (about 5% relative uncertainty in instrument supersaturation).

Size-resolved CCN activity is carried out using the Scanning Mobility CCN Analysis (SMCA) (Moore et al., 2010), where the DMA used for aerosol classification is operated in scanning voltage mode. This allows the concurrent determination of aerosol size distribution and size-resolved CCN activity over a voltage scan cycle. In this study, the complete range of dry particle size (20–850 nm) is scanned over three minutes. The CFSTGC was operated at a flowrate of $0.50\,1\,min^{-1}$ and a sheath-to-aerosol ratio of 10:1 (or 7.5:1). SMCA also provides the droplet distribution of activated CCN (measured in the optical particle counter of the CCN

instrument) as a function of their dry diameter. The dependence of droplet size on the supersaturation profile and dust dry particle size is used to study the dust activation kinetics.

2.3 Data analysis methodology

The measurement of D_{dry}, and corresponding s_c, is fitted with a power law function $s_c = CD_{dry}^x$. The experimental exponent, x_{exp} (Kumar et al., 2009b), is then compared against the exponent determined from fits of KT and FHH-AT to the data. The appropriateness of each theory is evaluated based on its ability to reproduce x_{exp}. According to KT, particles with appreciable hygroscopicity exhibit $x = -3/2$. In FHH-AT, x depends on the value of A_{FHH} and B_{FHH} but generally ranges between -0.80 and -1.20 (Kumar et al., 2009a). The same fitting procedure also determines the adsorption parameters A_{FHH} and B_{FHH} (for FHH-AT), and the hygroscopicity parameter κ (for KT).

B_{FHH} strongly affects the shape of the equilibrium curve and largely determines the existence and value of s_c and critical wet diameter, D_c (described as the wet diameter of the aerosol particle at the maximum of the equilibrium curve) (Kumar et al., 2009a). A_{FHH} also affects these parameters, but to a lesser extent than B_{FHH}. Figure 2 shows the relationship between D_{dry} and s_c for a range of B_{FHH} values computed at surface tension of water equal to 0.072 J m^{-2}, temperature equal to 298.15 K, and $A_{FHH} = 2.50$. Lower B_{FHH} values correspond to more hydrophilic dust. As B_{FHH} approaches 3.0, particles become less hydrophilic (with $x \rightarrow -1$), which corresponds to insoluble but wettable particles that follow the Kelvin equation. Similarly for KT, as κ decreases from $\kappa = 0.05$ to $\kappa = 0$ (Fig. 2) particles becomes less hygroscopic causing a decrease in the exponent from $x = -1.5$ to $x \rightarrow -1.0$. It can be seen from Fig. 2 that the slopes determined from KT (expressed in terms of κ) are much steeper than those determined from FHH-AT (expressed in terms of B_{FHH}). This suggests that the same particle type can exhibit two different s_c-D_{dry} exponent values if described by KT or FHH-AT.

Droplet activation kinetics of aerosol inside CFSTGC depends on the supersaturation profiles, residence time, water vapor uptake coefficient, dry particle size (Nenes et al., 2001; Roberts and Nenes, 2005; Lance et al., 2006), as well as the theory used to describe the equilibrium vapor pressure for the particle (KT or FHH-AT). Activation kinetics can be characterized by the difference in droplet size, ΔD_w, between dust CCN and $(NH_4)_2SO_4$ CCN with same s_c. A negative ΔD_w implies that mineral aerosol exhibits retarded activation kinetics (the converse is typically not observed). This technique is called threshold droplet growth analysis (TDGA) and has been successfully used by a number of in-situ and laboratory studies (Asa-Awuku et al., 2010; Padró et al., 2010).

We quantitatively describe the growth of dust by simulating the process of droplet nucleation and growth within
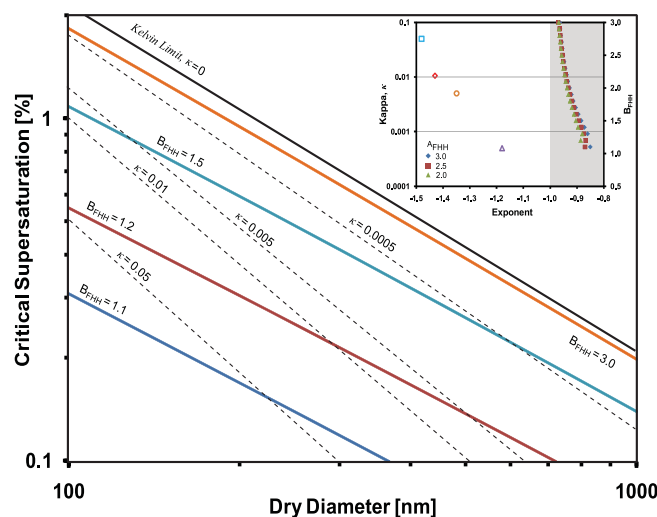

Fig. 2. s_c-D_{dry} lines for different values of B_{FHH} computed at $\sigma = 0.072$ J m^{-2}, $T = 298.15$ K and $A_{FHH} = 2.50$. Dashed lines indicate κ isolines determined at above conditions. Also shown in black thick line is the $\kappa = 0$, Kelvin curve. The inset figure shows experimental exponent as function of B_{FHH} and κ.

the CCN instrument using the comprehensive computational fluid dynamics model. We use the Lance et al. (2006) model, which numerically simulates the temporal and spatial distributions of velocity, pressure, temperature, and water vapor concentration throughout the growth chamber, considering the coupling of particle and gas phases through the release of latent heat and condensation/evaporation of water vapor onto the droplets. The kinetics of dust activation is then parameterized in terms of an effective uptake coefficient, which influences the mass transfer coefficient of water onto the dust CCN. Condensational growth of aerosol is computed based on a size-dependent mass transfer coefficient multiplied by the difference between gas-phase and equilibrium water vapor pressure (Nenes et al., 2001):

$$D_p \frac{dD_p}{dt} = \frac{s - s_{eq}}{\frac{\rho_w RT}{4 P_{H_2O}^\circ D_v' M_w} + \frac{\Delta H_v M_w}{4 k_a' T}\left(\frac{\Delta H_v \rho_w}{RT} - 1\right)} \tag{1}$$

where D_p is the droplet diameter, s is the local instrument supersaturation, ρ_w is the water density, M_w is the molar mass of water, R is the universal gas constant, T is the average column temperature, $P_{H_2O}^\circ$ is the equilibrium water vapor pressure, ΔH_v is the enthalpy of vaporization of water, D_v' is the diffusivity of water vapor in air modified for non continuum effects, and k_a' is the thermal conductivity of air modified for non continuum effects. Here D_v' is defined by Fukuta and Walter (1970) as:

$$D_v' = \frac{D_v}{1 + \frac{2 D_v}{\alpha_c D_p}\sqrt{\frac{2\pi M_w}{RT}}} \tag{2}$$

Table 1. Summary of Regional Dust Samples and Clays/Minerals analyzed in this study.

Sample	Abbreviation	Location/Supplier
Dust		
Niger	Niger	Sahel, 13°31′ N, 2°38′ E
East Asian Soil 1	Soil 1	Eastern edge of the Hexi Corridor
East Asian Soil 2	Soil 2	South-eastern edge of the Tengger Desert
East Asian Soil 3	Soil 3	Central Tengger Desert
East Asian Soil 4	Soil 4	South-eastern edge of the Taklamakan Desert
East Asian Soil 5	Soil 5	Southern edge of the Hunshandake Desert
Arizona Test Dust	ATD	Powder Technologies Inc.
Clay/Mineral		
Illite	Illite	Clay Mineral Society
Ca Montmorillonite	Ca Mont	Clay Mineral Society
Na Montmorillonite	Na Mont	Clay Mineral Society
Calcite	$CaCO_3$	OMYA
Quartz/Silica	SiO_2	GELEST

where D_v is the diffusivity of water vapor in air, α_c is the water vapor uptake coefficient. k'_a is given by:

$$k'_a = \frac{k_a}{1 + \frac{2k_a}{\alpha_T D_p \rho_a c_p}\sqrt{\frac{2\pi M_a}{RT}}} \quad (3)$$

where M_a is the mean molar mass of air, k_a is the thermal conductivity of air, ρ_a is the air density, c_p is the heat capacity of air, and α_T is thermal accommodation coefficient (equal to 1.0). For insoluble CCN activating according to FHH-AT, the equilibrium supersaturation of the droplet, s_{eq}, is given by Kumar et al. (2009a):

$$s_{eq} = \exp\left[\frac{4\sigma M_w}{RT\rho_w D_p} - A_{FHH}\left(\frac{D_p - D_{dry}}{2D_{H_2O}}\right)^{-B_{FHH}}\right] - 1 \quad (4)$$

where σ is the CCN surface tension at the point of activation (Pruppacher and Klett, 1997), D_{dry} is the dry CCN diameter, D_{H_2O} is the diameter of water molecule equal to 2.75 Å (Kumar et al., 2009a), and A_{FHH} and B_{FHH} are adsorption parameters constrained from the activation experiments.

The instrument model was initialized using the appropriate geometric dimensions and operating conditions of DMT CFSTGC (Lance et al., 2006). A computational grid of 200 cells in the radial and 200 cells in the axial direction were used in each simulation. A Lagrangian approach is used to determine CCN growth in the CFSTGC by Eq. (1), assuming the particles flow along streamlines occupied by the aerosol region of the chamber (determined from the sheath-aerosol ratio) and grow according to the local water vapor saturation ratio and temperature (Roberts and Nenes, 2005; Lance et al., 2006). The droplet diameter at the exit of the flow chamber is then compared against the measured droplet size distribution, following the binning scheme used in the optical detection of

the instrument. The value of uptake coefficient is then inferred by minimizing the discrepancy between predicted and observed droplet distributions in OPC.

3 Results and discussion

3.1 Effects of multiple charging and dust particle shapes

3.1.1 Correction for multiply charged particles in SMCA

To account for the effect of multiply charged particles in the activation curves and observed D_{dry}, we assume an equilibrium charge distribution for the particles entering the DMA and apply a correction algorithm as described in Moore et al. (2010). The correction algorithm determines the contribution from the multiply charged (+2, +3, +4, +5 and +6 charges) particles to the total particle counts in each size bin for the CN time series and rebins respective contributions to its "true" size bin. The same procedure is applied to the CCN time series. The inversion of the CN, CCN time series determines the activation fraction and hence D_{dry}. To ensure sufficient residence time for attaining equilibrium charge distribution inside the Kr-85 neutralizers, we determine the number of neutralizers beyond which the inverted size distribution does not change. Test results indicate that 3 Kr-85 neutralizers in series (with a total nominal activity of 10 mCi) were sufficient to completely neutralize the surface charges and attain the Boltzmann equilibrium distribution.

The impact of multiply charged particles is shown in Fig. 3, which presents the activation curves (with and without multiple charging corrections) at 0.30% supersaturation
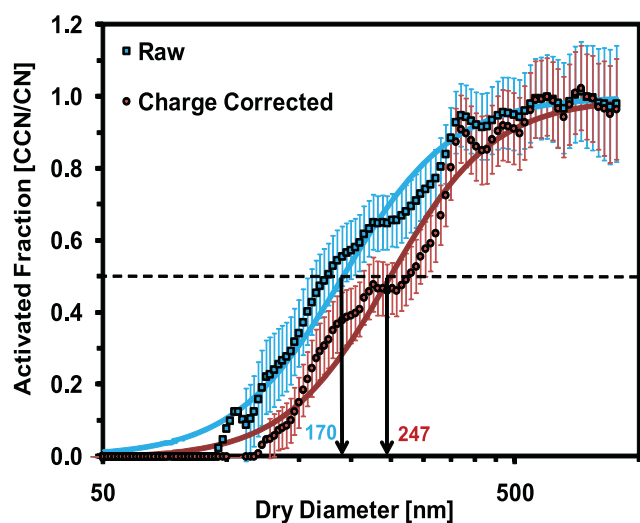
Fig. 3. Activation curves for Soil 2 at $s_c = 0.3\%$. Shown are inversions without (blue) and with multiple charge corrections (brown). Error bars represent uncertainty of activation efficiency as a result of counting efficiency and flow rate uncertainty at different diameters.

for aerosol generated from the Soil 2 sample. D_{dry} increases from ~170 nm to ~247 nm upon application of the multiple charge correction. The effect on D_{dry} is further enhanced at lower supersaturations (e.g., $s_c = 0.15\%$ and $s_c = 0.20\%$) that correspond to large particles with a pronounced probability of multiple charging. The uncertainty in the activation efficiency due to counting statistics uncertainty and flow rate variability (expressed as error bars in Fig. 3) were accounted for using the procedure of Moore et al. (2010).

3.1.2 Accounting for dust non-sphericity

Dust particles exhibit a variety of complex shapes that are difficult to measure or express in terms of a unique set of parameters or functions. Characterization of dust non-sphericity is often done by either (i) introducing a dynamic shape factor, χ, (defined as the ratio of drag force, F_D, experienced by the non-spherical particle to that experienced by a volume equivalent sphere when both move at the same velocity in the gas; e.g., DeCarlo et al., 2004), or (ii) providing an Aspect Ratio (AR), defined as the ratio of the longest dimension of particles to the orthogonal shortest length (width). Commonly, χ is obtained by tandem electrical mobility and aerodynamic particle sizing (e.g., DeCarlo et al., 2004; Kuwata and Kondo, 2009) and is an integrated measure of the three-dimensional particle shape. AR is measured with electron microscopy that reports two dimensional image projections of particles from which the longest dimension and width are determined (e.g., Kalashnikova and Sokolik, 2004).

Here we assess the effect of dust non-sphericity in CCN activity measurements by considering the range of values of

AR or χ reported in the literature for different types of mineral aerosol. A number of recent studies have reported measurements of AR values for species considered in this study. For instance, Chou et al. (2008) report a mean AR equal to 1.7 for Niger dust collected during the AMMA campaign, Kandler et al. (2009) report AR equal to 1.64 for Saharan dust collected over Spain, and Coz et al. (2009) report AR equal to 1.81 for African dust. The AR values for African soils are slightly higher compared to AR of 1.3–1.4 reported by Okada et al. (2001) for East Asian dust. AR can also vary with particle size (Wiegner et al., 2009). To account for this, we considered those values of AR that are most relevant for this study (i.e., particles less than 1 μm). Furthermore, the extent of non-sphericity can be affected by the aerosol generation method (Sullivan et al., 2010) which can give rise to very different particle morphologies from those generated with the dry soft-saltation technique used in this study. Some of the other techniques of aerosol generation include a fluidized bed (Koehler et al., 2009), dry dust generator (Herich et al., 2009), and atomization of a dust aqueous suspension (Koehler et al., 2009; Herich et al., 2009). All above factors can contribute to uncertainty in χ for similar aerosol types. For instances for ATD, Möhler et al. (2008) reported $\chi = 1.3$ while Endo et al. (1998) reported $\chi = 1.5$. Similarly for illite, Hudson et al. (2008) and Möhler et al. (2008) reported $\chi = 1.3 \pm 0.02$ and $\chi = 1.3$ respectively. For other clays and minerals analyzed in this study such as montmorillonite, Hudson et al. (2008) reported $\chi = 1.11 \pm 0.03$, while Hinds (1999) report a value of $\chi = 1.36$ for quartz.

In this study, we use the published range of dust non-sphericity. As most of the recent studies on African and Asian mineral dust aerosol have quantified dust non-sphericity based on AR, we initially started with the Fuchs (1964) approach to convert from AR to χ assuming mineral aerosol as a spheroid. However, we found that using the Fuchs (1964) approach results in much lower values of χ (~1.007–1.034) than those determined from direct measurements of χ (~1.11–1.50). According to Davies (1979), sand particles composed of a mixture of different minerals have a dynamic shape factor of 1.3–1.6. Therefore, in this study non-sphericity corrections are performed for all species considering $\chi = 1.3 \pm 0.2$ as this covers as possible values of measured χ. Further, we examine the importance of this uncertainty in χ (between $\chi = 1.1$ and $\chi = 1.5$) for dust-CCN measurements by evaluating its effect on x_{exp} and FHH parameters, A_{FHH} and B_{FHH}.

Size selection in this study is performed using the DMA that classifies a particle by its electric mobility. Electrical mobility can then be related to the physical diameter if the number of elementary charges per particle and χ are known (together with the strength of the electric field and other operational parameters in the DMA). Often χ is assumed unity. For mineral dust, however, $\chi > 1$ which translates into a larger drag force than expected for spherical particles; when neglected, the nonsphericity would eventually lead to

underestimation of the particle surface area. In this study, we account for dust non-sphericity by correcting for the surface area of the particle available for water vapor adsorption. This is performed by converting from electrical mobility diameter, D_m, to surface-area equivalent diameter, D_{se}, so that the CCN activity data is expressed in terms of the s_c-D_{se} relationship. By converting from D_{dry} to D_{se}, the aerosol physical size is expressed in terms of the characteristic length responsible for controlling surface water vapor adsorption. D_{se} is determined by converting the electrical mobility diameter (D_m), to particle volume equivalent diameter (D_{ve}), and from there to D_{se}.

Determining D_{ve} from D_m

D_{ve} is determined from D_m by iterative solution of the dynamic shape factor equation (DeCarlo et al., 2004):

$$\chi = \frac{D_m C(D_{ve})}{D_{ve} C(D_m)} \tag{5}$$

where $C(D_m)$ and $C(D_{ve})$ are the slip correction factors for D_m and D_{ve}, respectively. $C(D_m)$ and $C(D_{ve})$ can be approximated from the correlation of Willeke and Baron, (2001):

$$C(D_i) = 1 + \frac{2\lambda}{D_i}\left(1.142 + 0.558 \exp\left(-0.999\frac{D_i}{2\lambda}\right)\right) \tag{6}$$

where λ is the mean free path of the gas molecules and D_i corresponds to either of D_m or D_{ve}. Application of Eq. (5) to determine D_{ve} requires knowledge of χ.

Determining D_{se} from D_{ve}

When χ is known (or estimated), the correlation of Leith (1987) is used to relate χ, D_{se}, and D_{ve}:

$$\chi = \frac{1}{3}\left(\frac{D_n}{D_{ve}}\right) + \frac{2}{3}\left(\frac{D_{se}}{D_{ve}}\right) \tag{7}$$

where D_n is the diameter of the sphere whose projected area is equal to that of the particle normal to the direction of flow. For the DMA, $D_n = D_m$, hence Eq. (7) can be rearranged to express D_{se} as:

$$D_{se} = \frac{3\chi D_{ve} - D_m}{2} \tag{8}$$

Despite involved uncertainties, accounting for dust non-sphericity provides more realistic representation of dust particles as well as enables us to determine non-sphericity effects on the physics controlling the activation of insoluble dust particles.
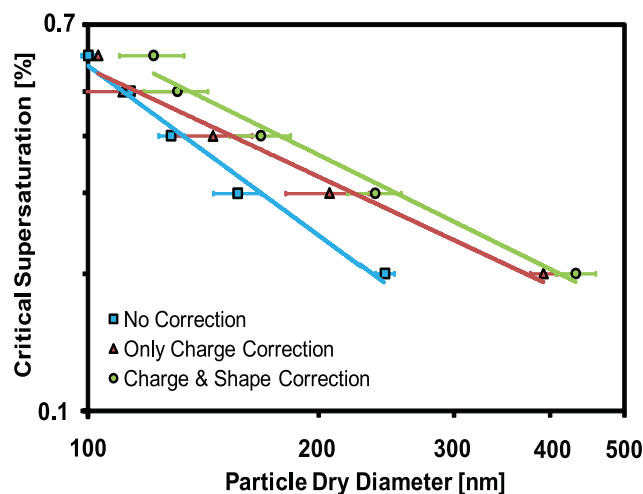

Fig. 4. CCN activation curves (s_c-D_{dry}) for ATD ($\chi = 1.3 \pm 0.2$) showing the effect of including charge and shape corrections on the raw data. Blue shows curve with no correction, brown shows the results with charging corrections and green shows curve after including both charge and shape corrections. Error bars represent experimental uncertainty and numerical uncertainty in D_{dry} at same instrument supersaturation.

3.1.3 Effect of charge and shape corrections on dust CCN activation

The largest change in dry critical activation diameter from multiple charging corrections is observed at the point of lowest supersaturation (corresponding to the largest activation diameters with highest probability of multiple charging). For all species considered in this study (regional dusts and clays/minerals), $\chi = 1.3$ was used to convert from charge corrected electrical mobility diameter, D_m to the shape corrected surface-area equivalent diameter, D_{se}. The error bars on D_{se} represent the range using $\chi = 1.1$ as the lower limit and $\chi = 1.5$ as the upper limit. We found that accounting for non-sphericity using $\chi = 1.3$, can result in an increase in activation diameters by up to 18–20% when converting from D_m to D_{se} using the procedure outlined above. Based on Fig. 4, as the final activation diameters (after including both charge and shape corrections) lie outside the experimental error bars (or region of experimental uncertainty) determined from the raw data, the essence of including the charge and shape corrections is justified and hence performed for all the samples studied here.

We also found that introducing both multiple charging and shape correction changes the dry activation diameters significantly and hence the exponents determined from the s_c-D_{dry} relationship. For example in the case of ATD, $x_{exp} = -1.23$ for the uncorrected data; after applying charge corrections, $x_{exp} = -0.78$; with shape and charge corrections, $x_{exp} = -0.82$. This is a very large and important difference, enough to shift the implied activation mechanism from a regime

where both FHH-AT and KT may be active ($x_{exp} = -1.23$) to a regime where FHH-AT dominates ($x_{exp} = -0.82$). This example emphasizes the importance of applying corrections (especially for multiple charges) for adequate interpretation of the activation data.

It is also noted that the effect of particle non-sphericity must be incorporated into the diameter used in the Kelvin term at the point of activation if only a few monolayers are adsorbed at activation (Romakkaniemi et al., 2001). We find that for all regional samples considered in our study, the number of adsorbed water vapor monolayers layers range from 100–500 at the point of activation. This implies that at the point of activation, non-spherical dust aerosol has sufficiently high water coverage so that the droplet shape is spherical, and, the molar volume and gas-liquid surface tension of the adsorbed H_2O approaches that for the bulk water.

3.2 Results of dust CCN activation measurements

The CCN activation curves for dry generated dust and mineral/clay samples are shown in Figs. 5 and 6, respectively. CCN activity is presented in terms of dry activation diameter (D_{se}, given by Eq. 8) against instrument supersaturation. The CCN activity data (points) are fit to a power law expression from which the experimental exponent, x_{exp}, is determined. The A_{FHH}, B_{FHH}, and corresponding exponent, x_{FHH}, were determined from fitting the FHH-AT model (lines) to the experimental data via least squares minimization. The dry generation method used in this study did not produce sufficient number concentrations of particles with sizes smaller than 100 nm. Hence the CCN activity is restricted to supersaturations 0.7% and below (corresponding to $D_{dry} \sim 100$ nm and above).

Figure 5 clearly demonstrates that dust aerosols are CCN at atmospherically relevant supersaturations. It also indicates that soft saltation technique can generate mineral dust in the fine mode (with D_{dry} between 100 nm and 500 nm) which may contribute to CCN. The measured D_{dry} for different dust samples are much larger than expected for $(NH_4)_2SO_4$, suggesting that dust has a lower CCN activation potential than what is expected for soluble aerosol like $(NH_4)_2SO_4$. Figure 5 suggests that dust aerosols collected from different regions of the globe can have different activation properties which are attributed to the physical properties, morphology and the chemical composition of the parent soils. The CCN activity comparisons amongst different regional dust samples indicate that East Asian soils have a range of CCN activity potentials with $B_{FHH} \sim 1.1 - 1.3$. In comparison, Niger Soil (representative of North African dust) and ATD (representative of North American dust) were found to exhibit less variability, with $B_{FHH} = 1.25 - 1.28$. The range in CCN activity of East Asian soils is most likely reflective of the compositional variability. Differences in CCN activity amongst samples collected in the same region likely reflect the chemical heterogeneity within the dust samples. We
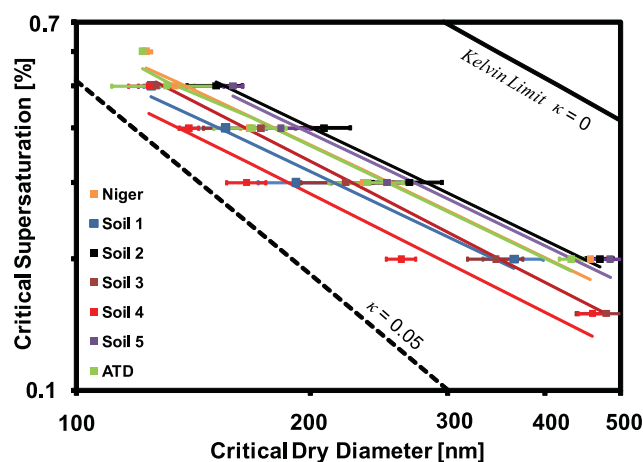

Fig. 5. CCN activation curves for different dust types presented in Table 1. Symbols show experimentally determined CCN activity and lines show FHH adsorption activation fits. Error bars represent measurement uncertainty in D_{dry}. Also shown in black thick line is the $\kappa = 0$, Kelvin curve. Black dashed line corresponds to $\kappa = 0.05$.

found that the experimental data (points) can be described by FHH-AT fits (lines) well, with $A_{FHH} \sim 2.25 \pm 0.75$ and $B_{FHH} \sim 1.20 \pm 0.10$ for all dust types considered in this study. A direct comparison of CCN activity against data published in the literature is done by expressing our results (for particles of a given dry diameter) in terms of a hygroscopicity parameter, κ. CCN activity results for regional soils, and minerals and clays indicate a $\kappa \leq 0.05$ for all samples considered in this study. It is also noted that the differences in values of the adsorption parameters determined in this study with those determined by Kumar et al. (2009b) for ATD, and likely arise from the application of multiple charge and dust non-sphericity corrections. Furthermore, the ATD experimental data used by Kumar et al. (2009b) in the predictions of adsorption parameters were taken from Koehler et al. (2009) that used a fluidized bed to generate aerosols, while in this study measurements were performed using a dry generation technique.

Figure 6 presents the CCN activity of all the minerals and clays considered. The activation diameters obtained for different dusts (Fig. 5) are within the range of those observed for different clays and minerals (Fig. 6). This suggests that dust CCN activity is controlled by adsorption of water onto the clay and mineral components in the dust samples. Comparison between CCN activities for different clays indicates montmorillonite (both Na and Ca rich) is more hydrophilic than illite, which agrees with the findings of Herich et al. (2009). Higher CCN activation potential for montmorillonite can be attributed to the mineralogy of the sample; the presence of unbounded Na and Ca cations allows water to penetrate the interlayer molecular space, which together with adsorption results in the clay swelling to several times its original volume. In the case of illite, the interlayer space
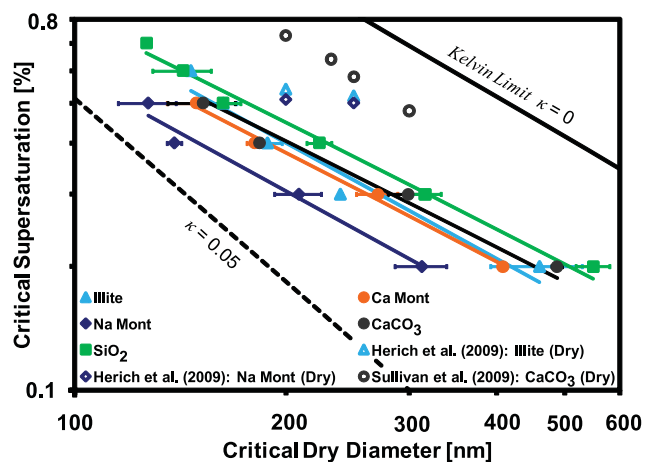
Fig. 6. CCN activation curves for different mineral types presented in Table 1. Symbols (filled) are experimentally determined CCN activity, and lines represent FHH adsorption activation fits. Open symbols represent data obtained from Sullivan et al., 2009, and Herich et al., 2009. Color scheme of open symbols identical to CCN activity observed with measurements in this study. Error bars represent measurement uncertainty in D_{dry}. Also shown in black thick line is the $\kappa = 0$, Kelvin curve. Black dashed line corresponds to $\kappa = 0.05$.

is mainly occupied by poorly hydrated potassium cations that prevent these clay types from expanding, thus reducing the amount of water that can adsorb on the surface and its CCN activation potential.

The CCN activity of SiO_2 and $CaCO_3$ was also measured (Fig. 6). As expected, SiO_2 was the least CCN active of species considered with $B_{FHH} = 1.36$ versus $B_{FHH} < 1.30$ for the other clays and minerals (Table 2). This is because the majority of the silica surface does not interact strongly with water vapor since physisorption occurs primarily on the limited number of silanol sites (Young, 1958). We also find that the charged-corrected activation curves in our study differ from published CCN activation data for $CaCO_3$ (Sullivan et al., 2009), montmorillonite, and illite (Herich et al., 2009). For example, charge-corrected activation curves for clays (illite and Na-montmorillonite) exhibited $\kappa = 0.02 - 0.04$, versus 0.002–0.003 in Herich et al. (2009). In addition, (OMYA) $CaCO_3$ in this study was found to exhibit multiple κ values, 0.02 at $s_c = 0.4\% - 0.5\%$ and 0.003–0.007 at $s_c = 0.2\%$–0.3%, higher than found by Sullivan et al. (2009) for (Solvay) $CaCO_3$ ($\kappa = 0.0011$). Our results for (OMYA) $CaCO_3$ at low s_c ($\kappa = 0.003 - 0.007$) compare well with results obtained for (Baker) $CaCO_3$ ($\kappa = 0.008$) (Sullivan et al., 2010). Similarly, we find a good comparison in CCN activity measurements based on κ values for regional dust samples considered in this study (for activation curves with and without multiple charging corrections) and past studies. For dry generated ATD (non-corrected), $\kappa = 0.04$ determined in this study compares well with non-corrected $\kappa = 0.025$ found by Koehler et al. (2009). Similarly, a good comparison for African dust

samples was found with charge-corrected $\kappa = 0.023$ (Herich et al., 2009) and non-corrected $\kappa = 0.054$ (Koehler et al., 2009) determined for Saharan Dust, and charge-corrected and non-corrected $\kappa = 0.02 - 0.04$ for Niger dust data.

The differences cited above for $CaCO_3$ can be attributed to factors such as sample-to-sample variability (as confirmed by Sullivan et al., 2010) and method of aerosol generation. The soft saltation technique may yield very different particles from studies using a custom-built dry dust generator (Herich et al., 2009) or fluidized bed (Koehler et al., 2009). Furthermore, the lack of charge correction (in previous studies) will provide activation curves sensitive to the aerosol size distribution (as it determines the fraction of multiply charged particles with same mobility diameter), so differences in the dust size distribution will lead to variable biases in D_{dry}. Unfortunately, absence of number size distributions of the CCN in the published studies precludes a conclusive attribution of these differences to multiple charging biases.

Table 2 shows the values of the experimental exponent, determined from the s_c-D_{dry} data for all dust samples and individual minerals/clays. The x_{exp} values determined in this study are much lower than those reported by Kumar et al. (2009b) that were determined from the experimental data of Koehler et al. (2009) and Sullivan et al. (2009). This is a result of experimental measurements performed in this study at much lower supersaturations, as well as the application of multiple charge and shape factor corrections to the activation curves that tend to further shift D_{dry} and x_{exp} (as illustrated in Fig. 4).

In Fig. 7, x_{FHH} is plotted against x_{exp} for all dust samples and individual minerals/clays. For $CaCO_3$, the value of x_{exp} from the uncorrected s_c-D_{dry} data equals -0.81. The value of x_{exp} after charge and shape correction reduces further to -0.75. As x_{exp} for $CaCO_3$ is outside the range of exponents that can be predicted by FHH-AT, x_{FHH} deviates from x_{exp} by more than 10%. For Na-montmorillonite, Ca-montmorillonite, Soil 1 and Soil 3, x_{FHH} is in excellent agreement with x_{exp} suggesting that the above can be parameterized using FHH-AT. This suggests that the CCN activity of clays is consistent with multilayer adsorption activation theory. In the case of illite, SiO_2, ATD, Niger, Soil 2, Soil 4, and Soil 5, x_{FHH} lies within the variability of x_{exp}, suggesting that FHH-AT also is an excellent description of CCN activity. Considering the uncertainty observed in experimental exponents (Fig. 7), it can be argued that the dust samples considered in this study are in excellent agreement with FHH-AT. Furthermore, x_{exp} for all samples are found to be between -0.80 and -1.20 (range relevant for adsorption activation as given by Kumar et al., 2009a) as well as between -0.75 (determined for $CaCO_3$) and -0.93 (determined for Na-montmorillonite) providing support that nucleation of freshly generated regional dust aerosols is controlled by water vapor adsorption on clays and minerals. This confirms the conclusions of Kumar et al. (2009b) that (i) using the KT framework for parameterizing dust-CCN interactions

Table 2. FHH parameters and exponent comparisons for different regional dusts and individual clays/minerals.

Sample	A_{FHH}	B_{FHH}	x_{exp}	x_{FHH}
Dust				
Niger	2.94 ± 0.06	1.27 ± 0.02	$-0.79 \pm 0.02 + (0.04)$	-0.87
Soil 1	2.94 ± 0.06	1.24 ± 0.02	$-0.84 \pm 0.02 + (0.05)$	-0.84
Soil 2	2.88 ± 0.11	1.30 ± 0.04	$-0.82 \pm 0.02 + (0.05)$	-0.85
Soil 3	1.36 ± 0.49	1.12 ± 0.03	$-0.92 \pm 0.03 + (0.05)$	-0.92
Soil 4	1.82 ± 0.39	1.13 ± 0.02	$-0.88 \pm 0.03 + (0.04)$	-0.89
Soil 5	2.91 ± 0.09	1.30 ± 0.03	$-0.78 \pm 0.03 + (0.05)$	-0.85
ATD	2.96 ± 0.03	1.28 ± 0.03	$-0.82 \pm 0.02 + (0.04)$	-0.83
Clay/Mineral				
Illite	1.02 ± 0.38	1.12 ± 0.04	$-0.92 \pm 0.03 + (0.05)$	-0.93
Ca Mont	2.06 ± 0.72	1.23 ± 0.04	$-0.88 \pm 0.02 + (0.05)$	-0.88
Na Mont	1.23 ± 0.31	1.08 ± 0.03	$-0.93 \pm 0.02 + (0.04)$	-0.93
$CaCO_3$	3.00 ± 0.04	1.30 ± 0.03	$-0.75 \pm 0.02 + (0.05)$	-0.85
SiO_2	2.95 ± 0.05	1.36 ± 0.03	$-0.82 \pm 0.03 + (0.04)$	-0.86

Values in parentheses indicate change in magnitude of x_{exp} from change in χ between 1.1 and 1.5.
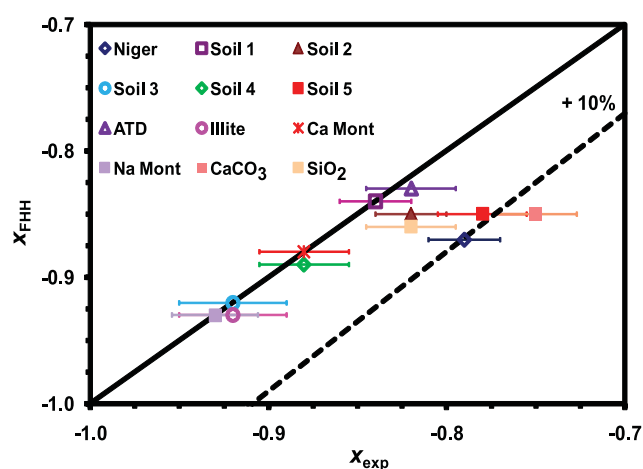

Fig. 7. Comparison of x_{exp} and x_{FHH} for dust and clay/mineral types presented in Table 1. Dashed line represents +10% deviation from the 1:1 line. Error bars represent deviation in x_{exp} due to the uncertainty in D_{dry}.

is inappropriate, and, (ii) adsorption effects must be included when describing the hygroscopic and CCN behavior of mineral aerosol.

It can also be seen from the insert in Fig. 2, that for KT to predict the correct exponent determined from the experimental s_c-D_{dry} relationships on dust and clays (shown as shaded region), the values of κ must be very low (less than 0.0005), much lower than those determined in previous studies (Koehler et al., 2009; Herich et al., 2009; Sullivan et al., 2009). On the contrary, FHH-AT can predict experimental exponents obtained from dust and clays s_c-D_{dry} relation-

ships (Table 2) using a single set of values for A_{FHH} and B_{FHH}. Furthermore, the predicted water vapor uptake under sub-saturated conditions is very low, and can explain the very low apparent hygroscopicity measured (using the hygroscopic tandem DMA technique) for dust aerosol (Herich et al., 2009). This strongly supports that FHH-AT describes fresh dust-CCN interactions better than KT for the samples considered in this study.

While the application of the shape factor corrections to CCN activation data changes the dry activation diameters considerably, it does so uniformly so that the exponent derived from the s_c-D_{dry} relationship (hence the implied activation physics) is not substantially affected. This can be seen from Table 2. Applying $\chi = 1.3 \pm 0.2$, changes x_{exp} by as little as 5% from charge corrected x_{exp}. Using $\chi = 1.3 \pm 0.2$ has a minor effect on dust hydrophilicity (indicated by a small range of B_{FHH}; Table 2). The omission of multiple-charging corrections to the activation curves, however, has a profound effect on the implied activation physics, as the dust appears significantly more CCN active than it really is.

3.3 Droplet growth kinetics

In addition to CCN activity, the optical particle counter of CFSTGC measures droplet sizes that can be used to explore CCN activation kinetics of mineral dust. This is carried out using TDGA, by comparing droplet diameter, D_w, from the sample CCN against that of $(NH_4)_2SO_4$ calibration aerosol with same critical supersaturation and maintaining identical instrument conditions (flow rates, pressure, and inlet temperature). If the droplet sizes from mineral aerosol are smaller than that observed from calibration aerosol (for conditions of identical instrument supersaturation, i.e., with same s_c), the
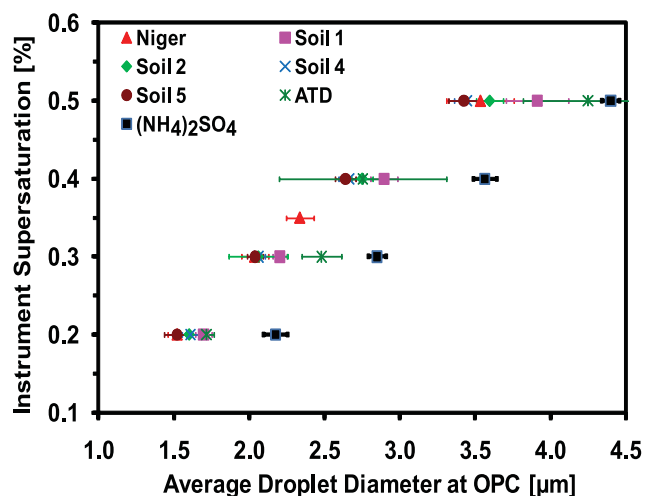
Fig. 8. Activated droplet sizes of mineral dust CCN with s_c equal to the instrument supersaturation shown as symbols. Error bars represent experimental uncertainty in droplet size as observed by the OPC at same instrument supersaturation.

Fig. 9. Activated droplet sizes of different minerals and clay CCN with s_c equal to the instrument supersaturation shown as symbols. Error bars represent experimental uncertainty in droplet size as observed by the OPC at same instrument supersaturation.

activation kinetics of mineral dust is likely slower than the calibration aerosol. However, if activated droplet sizes are indistinguishable (to within experimental uncertainty) from $(NH_4)_2SO_4$ droplet size, mineral dust exhibits the same activation kinetics as the reference aerosol.

Figure 8 presents the droplet diameters observed at OPC that are activated from regional dust aerosols as a function of instrument supersaturation. For comparison, droplet sizes are presented for pure $(NH_4)_2SO_4$ aerosol with s_c equal to the instrument supersaturation. It is evident that droplet growth for mineral aerosol at same s_c is lower than that determined for $(NH_4)_2SO_4$ calibration aerosol. The difference in outlet size suggests a delay in activation kinetics as both particles are exposed to the same supersaturation profile during their transit through the CFSTGC. This behavior is consistent with the slower time scales associated with water vapor adsorption (Kumar et al., 2009b). A similar behavior of reduced growth is also observed for different clays and minerals (Fig. 9).

Reduced growth at same s_c observed for the mineral aerosol inside the CFTSGC can be attributed to three potential factors: (i) different shape of the equilibrium curve (FHH-AT vs. KT), (ii) different mass transfer coefficient (or α_c) of water vapor to the growing droplet, and (iii) dry particle size. To compare the effect of theory (KT or FHH-AT) used to describe equilibrium vapor pressure, we simulated droplet sizes at the exit of CFSTGC column for different α_c and s_c. Simulations suggest that the size of activated droplets at the exit of the growth column, originating from particles activating at same s_c and with same α_c are almost identical, suggesting that the activation theory has an almost negligible effect on the final droplet size (not shown). Simulations (not shown) indicate that dry CCN size has a negligible effect
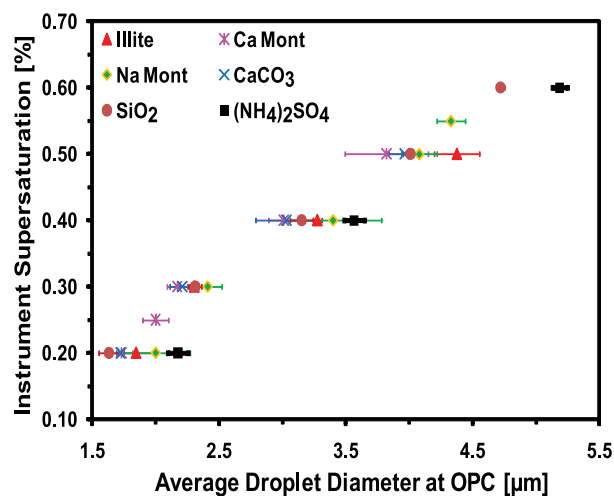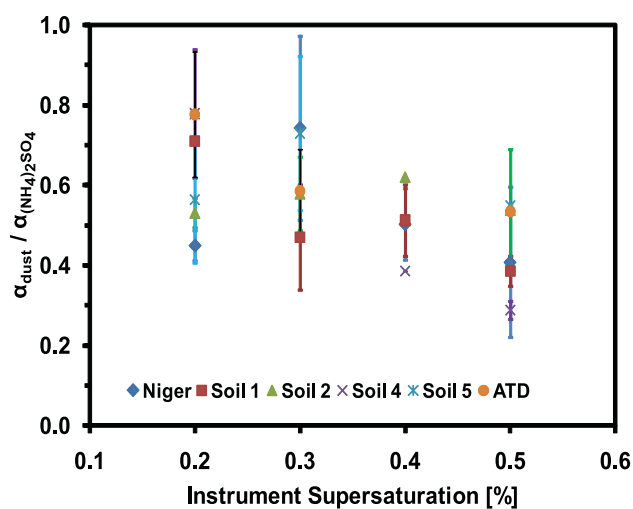

Fig. 10. Inferred water vapor uptake coefficients for the growth kinetics data of Fig. 8 normalized to that of $(NH_4)_2SO_4$ calibration aerosol as a function of different instrument supersaturation. Error bars represent experimental uncertainty in determination of water vapor uptake coefficients arising due to differences in droplet sizes measured by the OPC.

on final droplet sizes. Based on the above, the droplet size difference between dust CCN and $(NH_4)_2SO_4$ calibration aerosol is primarily driven by the intrinsic activation kinetics of the aerosol (which here is parameterized as difference in water vapor mass transfer coefficients (hence α_c)). This is consistent with a slower timescale associated with adsorption of additional multi-layers of water vapor than absorption of water from deliquesced aerosol (Seinfeld and Pandis, 2006; Pruppacher and Klett, 1997).

Data shown in Fig. 8 can be used to infer the water vapor uptake coefficient for dust by simulating dust CCN growth within the CFSTGC. Figure 10 shows values of α_c determined for different regional dust aerosols relative to $(NH_4)_2SO_4$. Compared to $(NH_4)_2SO_4$ calibration aerosol (that activates according to classical KT), mineral dust CCN grows to smaller droplet sizes that implies slower growth rate. When expressed in terms of α_c, it corresponds to an average 50% reduction in α_c. In absolute terms, if α_c of water upon deliquesced $(NH_4)_2SO_4$ aerosol is of order 0.2 (Davidovits et al., 2006), a 50% reduction would give α_c of water upon dust ~ 0.1. The α_c tends to decrease as instrument supersaturation increases; at the highest supersaturation, the amount of water adsorbed at D_c is much lower than for larger particles (low critical supersaturation). The kinetics of adsorption accelerates as the amount of adsorbed water increases (Pruppacher and Klett, 1997), so it is expected that α_c would decrease with particle size. The literature value of $(6.3 \pm 0.7) \times 10^{-2}$ determined for the water vapor uptake coefficient on mineral dust (Seisel et al., 2005) is in agreement with the inferred α_c from the highest critical supersaturation ($\alpha_c \sim 0.065$). The diversity of inferred uptake coefficients could also be related to the chemical heterogeneity between samples.

Retarded activation kinetics may have an impact on the activated droplet number in clouds that contain significant concentrations of dust CCN. It is shown by Nenes et al. (2002) that a reduced α_c affects the water uptake in the early stages of cloud formation (since droplets do not grow as rapidly); this leads to a higher parcel maximum supersaturation and hence a higher cloud droplet number. The extent of the impact depends on the vertical velocity, CCN concentration and the relative proportion of KT to FHH-AT particles. A thorough assessment will be the focus of a future study.

4   Summary

In this study, the CCN properties and droplet activation kinetics of aerosol generated from regional dust samples and individual minerals (clays, calcite, and quartz) were measured. The aerosols were generated dry in the lab, and properties were measured using the Scanning Mobility CCN Analysis (Moore et al., 2010). Including multiple charge corrections significantly increased D_{dry} and decreased x_{exp}. Dust non-sphericity was accounted for by converting from electrical mobility diameter, D_m, to surface area equivalent diameter such that the surface area available for adsorption can be accounted for. Non-sphericity corrections were accounted for by using the dynamic shape factor, $\chi = 1.3 \pm 0.2$ as this range covered published data for species considered in this study. It was found that while the application of the shape factor corrections to CCN activation data changes the dry activation diameters, it does so uniformly so that the magnitude of the exponent derived from the s_c-D_{dry} relationship (hence the

implied activation physics) is not substantially affected with a deviation of as low as 5%.

The x_{exp} for regional dust samples and mineral aerosols investigated in this study was found to be in excellent agreement with FHH-AT (mostly agreeing to within 10%) and one set of adsorption parameters ($A_{FHH} \sim 2.25 \pm 0.75$, $B_{FHH} \sim 1.20 \pm 0.10$). In contrast, KT cannot capture x_{exp} without a hygroscopicity parameter that exhibits very strong size-dependence. This confirms the assessment of Kumar et al. (2009b) and further supports that FHH-AT provides more realistic representation of fresh dust CCN activity than KT.

Using threshold droplet growth analysis, dust CCN was found to have a reduced growth compared to $(NH_4)_2SO_4$ calibration aerosol at the same instrument supersaturation. This implies slower activation kinetics of dust relative to $(NH_4)_2SO_4$ aerosol. These delays in activation by dust CCN, when parameterized in terms of the water vapor uptake coefficient, α_c, translates to a 30–80% (average = 50%) reduction in α_c (relative to the $(NH_4)_2SO_4$ aerosol).

The samples studied here are representative of major regional dust sources, and the adsorption activation parameters determined can be used to express their CCN potential in cloud droplet formation parameterizations developed by Kumar et al. (2009a). These parameterizations are valid for fresh dust in the dust source regions and for transported dust if it will not undergo significant atmospheric processing. A combined KT and FHH-AT framework, however, may be needed to accurately describe the CCN activity of aged dust, dry lakebed dust mixed with salts (e.g., Owens Lake, Texcoco, and Aral Sea), and more generally dust particles with significant amounts of soluble materials.

A major implication of this study is that freshly-emitted dust and mineral aerosols can act as CCN through the effects of water adsorption alone. In some cases, 100 nm dust particles can exhibit comparable hygroscopicity to an organic species with $\kappa \sim 0.05$ or a particle with $(NH_4)_2SO_4$ volume fraction of 10%. Dust particles in the Giant CCN (GCCN) size range will exhibit much lower apparent hygroscopicity because of their lower surface-to-volume ratio. Whether the effects of adsorption is sufficient to make freshly emitted dust GCCN act as a good collector drop is an open question left for a future study. Nevertheless, this study reshapes the conceptual notion of dust CCN activity to one where freshly emitted insoluble dust particles can have an appreciable hygroscopicity (that depends on their surface-to-volume ratio) which can be augmented through atmospheric processing.

Nomenclature

Symbol	Units	Description
s_c		Critical supersaturation
x		Power law exponent relating s_c and D_{dry}
D_{dry}	m	Dry CCN diameter
C	m^{-x}	Power law constant
x_{exp}		Experimental exponent
x_{FHH}		FHH-AT exponent
A_{FHH}		FHH adsorption isotherm parameter
B_{FHH}		FHH adsorption isotherm parameter
κ		Hygroscopicity parameter
D_c	m	Critical wet diameter
ΔT	K	Thermal gradient
s		Instrument supersaturation
ΔD_w	m	Droplet size difference at OPC
D_p	m	Droplet diameter
ρ_w	kg m^{-3}	Water density
M_w	kg mol^{-1}	Molar mass of water
R	J mol^{-1} K^{-1}	Universal gas constant
T	K	Average column temperature
$P_{H_2O}^\circ$	mbar	Equilibrium water vapor pressure
ΔH_v	J mol^{-1}	Enthalpy of vaporization of water
D_v'	m^2 s^{-1}	Diffusivity of water vapor in air modified for noncontinuum effects
D_v	m^2 s^{-1}	Diffusivity of water vapor in air
α_c		Water vapor uptake coefficient
k_a'	J m^{-1} s^{-1} K^{-1}	Thermal conductivity of air modified for non-continuum effects
M_a	kg mol^{-1}	Mean molar mass of air
k_a	J m^{-1} s^{-1} K^{-1}	Thermal conductivity of air
ρ_a	kg m^{-3}	Air density
c_p	J K^{-1}	Heat capacity of air
α_T		Thermal accommodation coefficient
s_{eq}		Droplet equilibrium supersaturation
σ	N m^{-1}	CCN surface tension
D_{H_2O}	m	Diameter of water molecule
F_D	N	Drag force
χ		Dynamic shape factor
AR		Aspect Ratio
D_m	m	Electrical mobility diameter
D_{se}	m	Surface-area equivalent diameter
D_{ve}	m	Volume equivalent diameter
$C(D_m)$		Slip correction factors for D_m
$C(D_{ve})$		Slip correction factors for D_{ve}
λ	m	Mean free path of the gas molecules
D_n	m	Diameter of the sphere whose projected area is equal to that of the particle normal to the direction of flow

References

Asa-Awuku, A., Nenes, A., Gao, S., Flagan, R. C., and Seinfeld, J. H.: Water-soluble SOA from Alkene ozonolysis: composition and droplet activation kinetics inferences from analysis of CCN activity, Atmos. Chem. Phys., 10, 1585–1597, doi:10.5194/acp-10-1585-2010, 2010.

Brunauer, S., Emmett, P. H., and Teller, E.: Adsorption of gases in multimolecular layers, J. Am. Chem. Soc., 60(2), 309–319, 1938.

Chou, C., Formenti, P., Maille, M., Ausset, P., Helas, G., Harrison, M., and Osborne, S.: Size distribution, shape, and composition of mineral dust aerosols collected during the African Monsoon Multidisciplinary Analysis Special Observation Period 0: Dust and Biomass-Burning Experiment field campaign in Niger, January 2006, J. Geophys. Res., 113, D00C10, doi:10.1029/2008JD009897, 2008.

Collins, W. D., Conant, W. C., and Ramanathan, V.: Earth radiation budget, clouds, and climate sensitivity, in: The chemistry of the atmosphere: Its impact on global change, edited by: Calvert, J. G., 207–215, Blackwell Scientific Publishers, Oxford, UK, 1994.

Coz, E., Gómez-Moreno, F. J., Pujadas, M., Casuccio, G. S., Lersch, T. L., and Artinano, B.: Individual particle characteristics of North African dust under different long-range transport scenarios, Atmos. Environ., 43, 1850–1863, 2009.

Davidovits, P., Kolb, C. E., Williams, L. R., Jayne, J. T., and Worsnop, D. R.: Mass accommodation and chemical reactions at gas-liquid interfaces, Chem. Rev., 106(4), 1323–1354, 2006.

Davies, C. N.: Particle-fluid interaction, J. Aerosol Sci., 10, 10477–10513, 1979.

DeCarlo, P. F., Slowik, J. G., Worsnop, D. R., Davidovits, P., and Jimenez, J. L.: Particle morphology and density characterization by combined mobility and aerodynamic diameter measurements. Part 1: Theory, Aerosol Sci. Technol., 38, 1185–1205, 2004.

DeMott, P. J., Sassen, K., Poellot, M. R., Baumgardner, D., Rogers, D. C., Brooks, S. D., Prenni, A. J., and Kreidenweis, S. M.: African dust aerosols as atmospheric ice nuclei, Geophys. Res. Lett., 30(14), 1732, doi:10.1029/2003GL017410, 2003.

Endo, Y., Chen, D.-R., and Pui, D. Y. H.: Effects of particle polydispersity and shape factor during dust cake loading on air filters, Powder Technol., 98(3), 241–249, 1998.

Field, P. R., Möhler, O., Connolly, P., Krämer, M., Cotton, R., Heymsfield, A. J., Saathoff, H., and Schnaiter, M.: Some ice nucleation characteristics of Asian and Saharan desert dust, Atmos. Chem. Phys., 6, 2991–3006, doi:10.5194/acp-6-2991-2006, 2006.

Forster, P., Ramaswamy, V., Artaxo, P., Berntsen, T., Betts, R., Fahey, D. W., Haywood, J., Lean, J., Lowe, D. C., Myhre, G., Nganga, J., Prinn, R., Raga, G., Schulz, M., and Van Dorland, R.: Changes in Atmospheric Constituents and in Radiative Forcing, in: Climate Change 2007: The Physical Science Basis. Contribution of Working Group I to the Fourth Assessment Report of the Intergovernmental Panel on Climate Change, edited by: Solomon, S., Qin, D., Manning, M., Chen, Z., Marquis, M., Averyt, K. B., Tignor, M., and Miller, H. L., Cambridge University Press, Cambridge, UK, and New York, NY, USA, 129–234, 2007.

Fuchs, N. A.: The Mechanics of Aerosols, Dover Publications, Inc., New York, USA, 37–43, 1964.

Fukuta, N. and Walter, L. A.: Kinetics of hydrometer growth from the vapor; spherical model, J. Atmos. Sci., 27, 1160–1172, 1970.

Ganor, E. and Foner, H: The mineralogical and chemical properties and behavior of Aeolian Saharan dust over Israel, in: The Impact of Desert Dust Across the Mediterranean, edited by: Guerzoni, S. and Chester, R., 163–172, Springer, New York, 1996.

Ganor, E. and Mamane, Y.: Transport of Saharan dust across the eastern Mediterranean, Atmos. Environ., 16, 581–587, 1982.

Hatch, C. D., Gierlus, K. M., Schuttlefield, J. D., and Grassian, V. H.: Water adsorption and cloud condensation nuclei activity

of calcite and calcite coated with model humic and fulvic acids, Atmos. Environ., 42, 5672–5684, 2008.

Herich, H., Tritscher, T., Wiacek, A., Gysel, M., Weingartner, E., Lohmann, U., Baltensperger, U., and Cziczo, D. J.: Water uptake of clay and desert dust aerosol particles at sub- and supersaturated water vapor conditions, Phys. Chem. Chem. Phys., 11, 7804–7809, doi:10.1039/b901585j, 2009.

Henson, B. F.: An adsorption model of insoluble particle activation: Application to black carbon, J. Geophys. Res., 112, D24S16, doi:10.1029/2007JD008549, 2007.

Hinds, W. C.: Aerosol Technology, John Wiley & Sons, Inc., New York, USA, 1999.

Hudson, P., Gibson, E. R., Young, M. A., Kleiber, P. D., and Grassian, V. H.: Coupled infrared extinction and size distribution measurements for several clay components of mineral dust aerosol, J. Geophys. Res., 113, D01201, doi:10.1029/2007JD008791, 2008.

Jeong, G. R. and Sokolik, I. N.: Effect of mineral dust aerosols on the photolysis rates in the clean and polluted marine environments, J. Geophys. Res., 112, D21308, doi:10.1029/2007JD008442, 2007.

Kandler, K., Schütz, L., Deutscher, C., Ebert, M., Hofmann, H., Jäckel, S., Jaenicke, R., Knippertz, P., Lieke, M., Massling, A., Petzold, A., Schladitz, A., Weinzierl, B., Wiedensohler, A., Zorn, S., and Weinbruch, S.: Size distribution, mass concentration, chemical and mineralogical composition and derived optical parameters of the boundary layer aerosol at Tinfou, Morocco, during SAMUM 2006, Tellus B, 61, 32–50, doi:10.1111/j.1600-0889.2008.00385.x, 2009.

Kalashnikova, O. V. and Sokolik, I. N.: Modeling the radiative properties of nonspherical soil-derived mineral aerosols, J. Quant. Specrtrocs. Ra., 87(2), 137–166, 2004.

Koehler, K. A., Kreidenweis, S. M., DeMott, P. J., Petters, M. D., Prenni, A. J., and Carrico, C. M.: Hygroscopicity and cloud droplet activation of mineral dust aerosol, Geophys. Res. Lett., 36, L08805, doi:10.1029/2009GL037348, 2009.

Köhler, H.: The nucleus in and the growth of hygroscopic droplets, Trans. Faraday Soc., 32(2), 1152–1161, 1936.

Kumar, P., Sokolik, I. N., and Nenes, A.: Parameterization of cloud droplet formation for global and regional models: including adsorption activation from insoluble CCN, Atmos. Chem. Phys., 9, 2517–2532, doi:10.5194/acp-9-2517-2009, 2009a.

Kumar, P., Nenes, A., and Sokolik, I. N.: Importance of adsorption for CCN activity and hygroscopic properties of mineral dust aerosol, Geophys. Res. Lett., 36, L24804, doi:10.1029/2009GL040827, 2009b.

Kuwata, M. and Kondo, Y.: Measurements of particle masses of inorganic salt particles for calibration of cloud condensation nuclei counters, Atmos. Chem. Phys., 9, 5921–5932, doi:10.5194/acp-9-5921-2009, 2009.

Lafon, S., Sokolik, I. N., Rajot, J. L., Caquineau, S., and Gaudichet, A.: Characterization of iron oxides in mineral dust aerosols: Implications to light absorption. J. Geophys. Res., 111, D21207, doi:10.1029/2005JD007016, 2006.

Lance, S., Medina, J., Smith, J. N., and Nenes, A.: Mapping the operation of the DMT continuous flow CCN counter, Aerosol Sci. Tech., 40, 242–254, 2006.

Leith, D.: Drag on nonspherical objects, Aerosol Sci. Tech., 6, 153–161, 1987.

Levin, Z., Ganor, E., and Gladstein, V.: The effects of dust particles coated with sulfate on rain formation in the Eastern Mediterranean, J. Appl. Meteorol., 35, 1511–1523, 1996.

Möhler, O., Benz, S., Saathoff, H., Schnaiter, M., Wagner, R., Schneider, J., Walter, S., Ebert, V., and Wagner, S.: The effect of organic coating on the heterogeneous ice nucleation efficiency of mineral dust aerosols, Environ. Res. Lett., 3, 8 pp., 2008.

Moore, R., Nenes, A., and Medina, J.: Scanning Mobility CCN Analysis – A method for fast measurements of size resolved CCN distributions and activation kinetics, Aerosol Sci. Tech., 44, 861–871, 2010.

Nenes, A., Ghan, S. J., Abdul-Razzak, H., Chuang, P. Y., and Seinfeld, J. H.: Kinetic limitations on cloud droplet formation and impact on cloud albedo, Tellus, 53B, 133–149, 2001.

Nenes, A., Charlson, R. J., Facchini, M. C., Kulmala, M., Laaksonen, A., and Seinfeld, J. H.: Can chemical effects on cloud droplet number rival the first indirect effect?, Geophys. Res. Lett., 29(17), 1848, doi:10.1029/2002GL015295, 2002.

Okada, K., Heintzenberg, J., Kai, K., and Qin Y.: Shape of atmospheric mineral particles collected in three Chinese arid-regions, Geophys. Res. Lett., 28(16), 3123–3126, doi:10.1029/2000GL012798, 2001.

Padró, L.T., Tkacik, D., Lathem, T., Hennigan, C., Sullivan, A. P., Weber, R. J., Huey, L. G., and Nenes, A.: Investigation of CCN relevant properties and droplet growth kinetics of water-soluble aerosol fraction in Mexico City, J. Geophys. Res, 115, D09204, doi:10.1029/2009JD013195, 2010.

Petters, M. D. and Kreidenweis, S. M.: A single parameter representation of hygroscopic growth and cloud condensation nucleus activity, Atmos. Chem. Phys., 7, 1961–1971, doi:10.5194/acp-7-1961-2007, 2007.

Petters, M. D., Prenni, A. J., Kreidenweis, S. M., and DeMott, P. J.: On measuring the critical diameter of cloud condensation nuclei using mobility selected aerosol, Aerosol Sci. Tech., 41, 907–913, 2007.

Pitzer, K. S. and Mayorga, G.: Thermodynamics of electrolytes. II. Activity and osmotic coefficients for strong electrolytes with one or both ions univalent, J. Phys. Chem., 77(19), 2300–2308, 1973.

Prospero, J. M.: Long-range transport of mineral dust in the global atmosphere: Impact of African dust on the environment of the southeastern United States, P. Natl. Acad. Sci. USA, 96, 3396–3403, 1999.

Pruppacher, H. R. and Klett, J. D.: Microphysics of clouds and precipitation 2nd ed., Kluwer Academic Publishers, Boston, MA, 1997.

Roberts, G. and Nenes, A.: A continuous-flow streamwise thermal gradient CCN chamber for atmospheric measurements, Aerosol Sci. Tech., 39, 206–221, 2005.

Romakkaniemi, S., Hämeri, K., Väkevä, M., and Laaksonen, A.: Adsorption of water on 8–15 nm NaCl and $(NH_4)_2SO_4$ aerosols measured using an ultrafine tandem differential mobility analyzer, J. Phys. Chem. A, 105, 8183–8188, 2001.

Rose, D., Gunthe, S. S., Mikhailov, E., Frank, G. P., Dusek, U., Andreae, M. O., and Pöschl, U.: Calibration and measurement uncertainties of a continuous-flow cloud condensation nuclei counter (DMT-CCNC): CCN activation of ammonium sulfate and sodium chloride aerosol particles in theory and experiment, Atmos. Chem. Phys., 8, 1153–1179, doi:10.5194/acp-8-1153-2008, 2008.

Rosenfeld, D., Rudich, Y., and Lahav, R.: Desert dust suppressing precipitation: A possible desertification feedback loop, P. Natl. Acad. Sci. USA, 98(11), 5975–5980, 2001.

Schuttlefield, J. D., Cox, D., and Grassian, V. H.: An investigation of water uptake on clays minerals using ATR-FTIR spectroscopy coupled with quartz crystal microbalance measurements, J. Geophys. Res., 112, D21303, doi:10.1029/2007JD008973, 2007.

Seisel, S., Pashkova, A., Lian, Y., and Zellner, R.: Water uptake on mineral dust and soot: A fundamental view of hydrophilicity of atmospheric particles?, Faraday Discuss., 130, 437–451, 2005.

Seinfeld, J. H. and Pandis, S. N.: Atmospheric Chemistry and Physics, John Wiley, New York, USA, 767–773, 2006.

Sokolik, I. N., Winker, D. M., Bergametti, G., Gillette, D. A., Carmichael, G., Kaufman, Y. J., Gomes, L., Schuetz, L., and Penner, J. E.: Introduction to special section: Outstanding problems in quantifying the radiative impacts of mineral dust, J. Geophys. Res., 106(D16), 18015–18027, 2001.

Sorjamaa, R. and Laaksonen, A.: The effect of H_2O adsorption on cloud drop activation of insoluble particles: a theoretical framework, Atmos. Chem. Phys., 7, 6175–6180, doi:10.5194/acp-7-6175-2007, 2007.

Sullivan, R. C., Moore, M. J. K., Petters, M. D., Kreidenweis, S. M., Roberts, G. C., and Prather, K. A.: Effect of chemical mixing state on the hygroscopicity and cloud nucleation properties of calcium mineral dust particles, Atmos. Chem. Phys., 9, 3303–3316, doi:10.5194/acp-9-3303-2009, 2009.

Sullivan, R. C., Moore, M. J. K., Petters, M. D., Kreidenweis, S. M., Qafoku, O., Laskin, A., Roberts, G. C., and Prather, K. A.: Impact of particle generation method on the apparent hygroscopicity of insoluble mineral particles, Aerosol Sci. Tech., 44, 10, 830–846, 2010.

Twohy, C. H., Kreidenweis, S. M., Eidhammer, T., Browell, E. V., Heymsfield, A. J., Bansemer, A. R., Anderson, B. E., Chen, G., Ismail, S., DeMott, P. J., and Van Den Heever, S. C.: Saharan dust particles nucleate droplets in eastern Atlantic clouds, Geophys. Res. Lett., 36, L01807, 1–6, doi:10.1029/2008GL035846, 2009.

Twomey, S.: Pollution and the planetary albedo, Atmos. Environ., 8, 1251–1256, 1974.

Wiegner, M., Gasteiger, J., Kandler, K., Weinzierl, B., Rasp, K., Esselborn, M., Freudenthaler, V., Heese, B., Toledano, C., Tesche, M., and Althausen, D.: Numerical simulations of optical properties of Saharan dust aerosols with emphasis on linear depolarization ratio, Tellus, 61B, 180–194, 2009.

Willeke, K. and Baron, P. A.: Aerosol Measurement: Principles, Techniques, and Applications. (2nd ed.). New York: John Wiley & Sons, Inc., 2001.

Young, G. J.: Interaction of water vapor with silica surfaces, J. Colloid Sci., 13(1), 67–85, 1958.